Journal Name

ARTICLE

Benzene-1,3,5-tricarboxamide *n*-alkyl ester and carboxylic acid derivatives: Tuneable structural, morphological and thermal properties

Received 00th January 20xx,
Accepted 00th January 20xx

DOI: 10.1039/x0xx00000x

www.rsc.org/

Amy D. Lynes,[a*] Chris S. Hawes,[a] Edward N. Ward,[b] Benjamin Haffner,[c] Matthias Mobius,[c] Kevin Byrne,[d] Wolfgang Schmitt,[d] Robert Pal[b] and Thorfinnur Gunnlaugsson[a*]

A family of five benzene-1,3,5-tricarboxamide **(BTA)** compounds with varied side arm functionality [alkyl: n =3, 4 and 5 chains; and ester and carboyxic acids) is reported. Investigations into their self-assembly behaviour revealed the extent to which minor changes in the side arm functionality can affect the structures formed. The carboxylic acid derivatives have a tendency to form gels, while the ester derivatives instead form crystalline phases with associated thermotropic phase transitions. The influence of the side chain length and terminal functional group is rationalised by a combination of single crystal X-ray diffraction studies and examinations of the bulk material properties.

Introduction

The study of supramolecular soft materials, and in particular, the correlation of structural features and the chosen self-assembly pathways of the chemical constituents with the properties of the bulk materials, is a research area of great current importance.[1, 2] Especially attractive synthetic platforms in such studies are those whose structures can be readily and systematically modified from a common core, with retention of the key modes of intermolecular interaction.[2] Owing to their symmetry and relatively simple structure, aggregation modes, and the vast range of possible derivatives, benzene-1,3,5-tricarboxamides (**BTAs**) have been a popular choice for application in supramolecular and nanomaterial chemistry.[3-9] Numerous studies into the self-assembly properties of **BTA**-derived structures and their supramolecular polymerization have been carried out, especially by Palmans, Meijer and co-workers.[8, 9, 10, 11] We have recently focused our efforts on the use of **BTA**-based ligands in the generation of functional soft materials such as lanthanide and transition metal ion based metallogels.[12] We have also employed the **BTA** unit in the generation of tripodal anion receptors[13] and *N*-methyl **BTA** derived platforms for the formation of anion-directed self-assembled cages and self-sorting assemblies.[14] Liquid-crystalline display technologies and various biomedical applications of **BTA** derivatives have also attracted significant interest in recent times.[3, 15, 16] In these systems, it has been widely reported that the nature of the side chains attached to the **BTA** core strongly influences the nature of self-assembly and the physical properties of the resulting materials in solution.[3, 11, 16] This has also been seen in several crystallographic studies where the hydrogen bonding between the amide groups of adjacent molecules dictates the organisation of the structures, with differences in packing of the molecules further observed due to variation of the side chain length.[3, 6, 16]

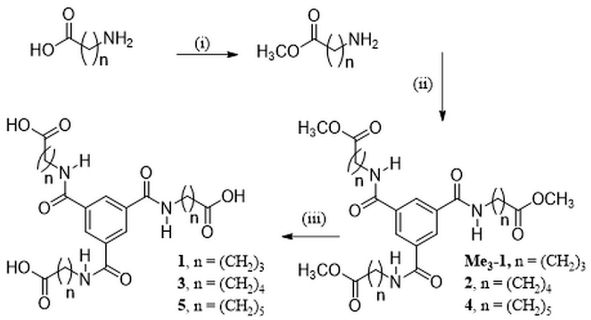

Scheme 1 (i) $SOCl_2$, CH_3OH, rt. (ii) Et_3N, DCM, 1,3,5-benzene tricarbonyl trichloride, Ar(g), rt. (iii) NaOH, CH_3OH, rt.

The tendency for **BTA** derivatives to form highly ordered one-dimensional hydrogen-bonded superstructures is a property lending itself well to the formation of several particular classes of soft materials.[6] For example, columnar **BTA** aggregates are well-suited to the formation of discotic liquid crystalline (LC) mesophases.[17] Individual columns also

[a] *School of Chemistry and Trinity Biomedical Sciences Institute (TBSI), The University of Dublin, Trinity College Dublin, Dublin 2, Ireland. gunnlaut@tcd.ie and lynesa@tcd.ie.*
[b] *Department of Chemistry, Durham University, South Road, Durham, DH1 3LE (UK).*
[c] *Sami Nasr Institute of Advanced Materials (SNIAM), School of Physics, The University of Dublin, Trinity College Dublin, Dublin 2, Ireland.*
[d] *School of Chemistry, Centre for Research on Adaptive Nanostructures and Nanodevices (CRANN), The University of Dublin, Trinity College Dublin, Dublin 2, Ireland.*
Electronic Supplementary Information (ESI) available: Thermogravimetric analysis plots, additional DSC data, NMR spectra, X-ray powder diffraction patterns and additional figures. See DOI: 10.1039/x0xx00000x

possess dipoles parallel to the director axis by virtue of the directional hydrogen bonding present. Such stacks can be addressed by an external field.[17] The formation of such phases under wide and accessible temperature ranges is largely favoured by long and weakly interacting side chains, particularly in the cases of asymmetric substitution of the three side groups.[4, 18] The alignment of **BTA** derivatives into one-dimensional aggregates is also conducive to the formation of supramolecular gels from solutions. In such materials – typically formed from **BTA** derivatives with chains containing additional hydrogen bonding groups or other supramolecular tectons – the aggregates take the form of an interconnected network of fibres or bundles. These are than capable of supporting the encapsulated solvent into robust, solid-like materials. The formation of hydrogels based on the **BTA** core substituted with *p*-carboxyphenyl side arms was recently reported by Schmidt *et al.*, with the gels found to be fully pH-reversible and thermostable up to 100°C.[19] Another report on the influence of side chain on structure and function was published by Haldar *et al.*[5] A **BTA** containing three L-methionine side chains was found to self-assemble in the classical threefold amide-amide hydrogen bonds and π-π stacking to form columnar structures. On the other hand, the tyrosine analogue, with additional hydrogen bonds and steric hindrance, did not show the classical threefold intermolecular amide bonding. Given our interest in this area of research, we set out to investigate the effect that small structural changes would have on the **BTA** core and its function. Herein, we report the synthesis, structural, physical and thermal properties of **1-5**, Scheme 1. These **BTA** derivatives, were synthesized in two to three steps, and contain either ester or carboxylic acid functional groups. We show that small changes in the spacer length ($3 < n < 5$) between the **BTA** core and the carbonyl functionalities, have a major effect on the self-assembly properties of these **BTA** structures on their resulting macroscopic properties.

Experimental

Materials and Methods

All reagents and solvents were purchased from Sigma-Aldrich, Fisher Scientific or TCI Ltd, were of reagent grade or better, and were used without further purification unless otherwise stated. Where necessary, solvents were dried over activated alumina using an Innovative Technology PureSolv solvent purification system. Electrospray ionisation mass spectra were recorded on a Mass Lynx NT V 3.4 on a Waters 600 controller connected to a 996 photodiode array detector with HPLC-grade CH_3CN or CH_3OH as carrier solvents. Infrared spectra were recorded in the range 4000-650 cm^{-1} on a Perkin-Elmer Spectrum One FT-IR spectrometer equipped with a Universal ATR sampling accessory. NMR data were recorded on a Bruker-DPX-400-Avance spectrometer (400.13 (^{1}H) and 100.6 (^{13}C) MHz) and on a Bruker AV-600 spectrometer (600.13 (1H) and 150.2 (13C) MHz) in commercially available deuterated solvents. Chemical shifts are reported in ppm relative to SiMe4 (= 0 ppm) and referenced relative to the internal solvent signals. Data were processed with Bruker Win-NMR 5.0, Topspin and MestReNova softwares. Melting point measurements were carried out using an electrothermal 1A900 melting point apparatus in an unsealed capillary tube. Elemental analysis was carried out on Exter Analytical CE440 elemental analyser at the microanalysis laboratory, School of Chemistry and Chemical Biology, University College Dublin. Thermogravimetric (TGA) analysis was carried out with a Perkin-Elmer Pyris 1 thermogravimetric analyser. Samples were spread on alumina crucibles and heated under nitrogen purge flow of 20 ml/min at a heating rate of 5 °C/min. The thermal phase transitions of each compound were examined using a Perkin Elmer Diamond Differential Scanning Calorimeter (DSC). Samples were prepared in crimped aluminium sample pans of 50μL capacity, with equivalent reference pans. Heating and cooling cycles were carried out at heating/cooling rates of 2 °C/min in the appropriate temperature range, with 5 minute equilibration times at the end of each temperature scan. All data are shown with endotherms upwards. A (BX53) cross polarising microscope equipped with XC50 camera and Linkam scientific instruments LTS420 temperature controlled stage equipped with Stream Basic software was used for the polarised optical microscopy images. Gas adsorption isotherms were measured using a Quantachrome Autosorb IQ gas sorption analyser. Chemically pure (CP) grade He, N_2, H_2 and CO_2 gases were used for the measurements. Rheological measurements were carried out with a Anton Paar MCR 301 rheometer using a plate–plate geometry.

Gel preparation and Imaging

The gels were prepared by dissolving the compounds in the appropriate solvent mixture at the specified concentrations, with gentle heating used to aid dissolution. Gelation occurred upon cooling the homogeneous solutions. The morphology of the gels were studied using a Carl Zeiss Ultra SEM, with the samples deposited on silicon wafers with a thick silicon dioxide layer. Prior to imaging, all samples were coated with a conductive layer of Pd/Au using a Cressington 208Hr high resolution sputter coater.

X-Ray crystallography and powder diffraction

Structural and refinement parameters are presented in Table 1. All diffraction data were collected using a Bruker APEX-II Duo dual-source instrument using microfocus Cu Kα (λ = 1.54178 Å) radiation. Datasets were collected using ω and ϕ scans with the samples immersed in oil and maintained at a constant temperature of 100 K using a Cobra cryostream. The data were reduced and processed using the Bruker APEX suite of programs.[20] Multi-scan absorption corrections were applied using SADABS.[21] The diffraction data were solved using SHELXT and refined by full-matrix least squares procedures using SHELXL-2015 within the OLEX-2 GUI.[22] The functions minimized were $\Sigma w(F^2_o-F^2_c)$, with $w=[\sigma^2(F^2_o)+aP^2+bP]^{-1}$, where

P=[max(F_o)^2+2F^2_c]/3. All non-hydrogen atoms were refined with anisotropic displacement parameters. All carbon-bound hydrogen atoms were placed in calculated positions and refined with a riding model, with isotropic displacement parameters equal to either 1.2 or 1.5 times the isotropic equivalent of their carrier atoms. Where appropriate and as discussed in the text, the positions of hydrogen atoms involved in hydrogen bonding interactions were refined to provide the best fit for the residual Fourier peaks and assigned a U_{iso} value equal to 1.5 times that of the nearest associated atom, with the appreciation that the exact positions of these atoms cannot be meaningfully inferred from X-ray diffraction data. Specific refinement strategies are outlined in the text and also in the refine_special_details section of the combined crystallographic information file (cif). CCDC 1503992-1503995. X-ray powder diffraction patterns were collected using a Bruker D2 Phaser instrument with Cu Kα radiation (λ = 1.5418 Å). Samples were ground and mounted on silicon sample holders, and data were collected in the 2θ range 5 – 55° at room temperature.

[Table 1]

Synthesis

*Synthesis of the **BTA** esters trimethyl 5, 5', 5''-((benzene-1,3,5-tri(carboxamide)) tris pentanoate **2** and trimethyl 6, 6', 6''-((benzene-1,3,5- tri(carboxamide)) tris hexanoate* **4**

The appropriate alkylamino-ester (15 mmol for **2** and 10 mmol for **4**) was dissolved in anhydrous DCM (50 mL) and cooled in ice, before addition of Et_3N (3 equivalents) dropwise. The solution was stirred under argon and allowed reach room temperature before addition of 1, 3, 5-Benzenetricarbonyl trichloride. The mixture was stirred for 24 hr at room temperature under argon. Solution was washed with $NaHCO_3$ solution in H_2O three times, with organic layer collected and evaporated to reveal a white solid which was dried *in vacuo.* Product was purified by silica column chromatography.

Trimethyl 5, 5', 5''-((benzene-1,3,5- tri(carboxamide)) tris pentanoate 2: Yield 77%; mp 89-90 ˚C; ^{1}H NMR (DMSO-d_6, 600 MHz, δ) 8.68 (t, *J*= 5.5 Hz, 3H, NH), 8.36 (s, 3H, Aromatic), 3.58 (s, 9H, Me), 3.28 (overlapping with H_2O signal, 6H, 1-CH_2), 2.35 (t, *J*= 7.1 Hz, 6H, 4-CH_2), 1.56 (m, 12H, 2-CH_2, 3-CH_2). ^{13}C NMR (DMSO-d_6, 150 Hz, δ) 173.26 (COOMe), 163.43 (CONH), 135.06 (Aromatic-chain), 128.3 (Aromatic), 51.17 (Me), 32.91 (C4), 28.43 (C1), 21.92 (C2, C3). Found: C, 58.98; H, 7.18; N, 7.64. Calc. for $C_{27}H_{39}N_3O_9$: C, 59.0; H, 7.15; N, 7.65%. HRMS-ESI$^+$ (*m/z)* : $[M+H]^+$ calcd for $C_{27}H_{40}N_3O_9$, 550.2686, found 550.2767. IR ν_{max} (cm^{-1}): 3224m, 3066m, 2955m, 2875w, 1736s, 1636s, 1561s, 1470m, 1434m, 1414m, 1327m, 1311m, 1245m, 1188m, 1106m, 1084m, 1028w, 977m, 882w, 744s, 664s, 597w.

Trimethyl 6, 6', 6''-((benzene-1,3,5-tri(carboxamide)) tris hexanoate 4: Yield 80%; mp 84 ˚C. ^{1}H NMR (DMSO-d_6, 600 MHz, δ) 8.67 (bs, 3H, NH), 8.35 (s, 3H, 6-CH_2), 3.57 (s, 9H, OMe), 3.27 (m, 6H, 1-CH_2), 2.31 (t, 6H, *J* = 7.6 Hz, 5-CH_2), 1.55 (dd, 12H, *J* = 15.1, 7.6 Hz, 2-CH_2, 4-CH_2), 1.32 (m, 6H, 3-CH_2). ^{13}C NMR (DMSO-d_6, 150 Hz, δ) 173.37 (COOMe), 165.44 (CONH), 135.13 (Aromatic), 128.32 (Aromatic), 51.21 (OMe), 33.22 (C1), 28.71 (C5), 25.93 (C2, C4), 24.19 (C3). Found: C, 60.98; H, 7.73; N, 7.11. Calc. for $C_{30}H_{45}N_3O_9$: C, 60.88; H, 7.67; N, 7.10%. HRMS-ESI$^+$ (*m/z)* : $[M+H]^+$ calcd for $C_{30}H_{46}N_3O_9$, 592.3156, found 592.3325. IR ν_{max} (cm^{-1}): 3232m, 3069m, 2939m, 2865w, 1736s, 1636s, 1560s, 1464w, 1435m, 1417w, 1373w, 1292m, 1233m, 1188w, 1164s, 1107m, 1008w, 907w, 883w, 794w, 732m, 579w.

*Synthesis of carboxylic acid derivatives trimethyl 4, 4', 4''-((benzene-1,3,5- tri(carboxamide)) tris butanoic acid **1**, trimethyl 5, 5', 5''-((benzene-1,3,5- tri(carboxamide)) tris pentanoic acid **3**, and trimethyl 6, 6', 6''-((benzene-1,3,5-tri(carboxamide)) tris hexanoic acid **5***

The corresponding ester derivative (1.9 mmol in the case of **1**, **3** and 0.7 mmol in the case of **5**) was dissolved in 5 ml CH_3OH, cooled on ice and 5 equivalents of NaOH was added dropwise. The resulting solution was left to stir at room temperature for 4 hr. Acetic acid was added dropwise until the formation of a white precipitate occurred. This was then filtered and washed with H2O, with the resulting white solid dried in vacuo. The synthesis of **5** was previously reported using a similar method[23].

Trimethyl 4, 4', 4''-((benzene-1,3,5- tri(carboxamide)) tris butanoic acid 1: Yield 87%; mp 185 ˚C. 1H NMR (DMSO-d6, 600 MHz, δ) 12.08 (s, 1H, OH), 8.71 (t, J = 5.3 Hz, 3H, NH), 8.38 (s, 3H, Aromatic), 3.31 (overlapping with H_2O signal, 1-CH2), 2.31(t, J = 7.3 Hz, 6H, 3-CH2), 1.79 (quin, J = 7.3 Hz, 6H, 2-CH2). 13C NMR (DMSO-d6, 150 Hz, δ) 174.7 (COOMe), 166.1 (CONH), 135.5 (Aromatic chain), 128.9 (Aromatic), 39.3 (C3), 31.6 (C1), 24.9 (C2). Found: C, 52.21; H, 6.09; N, 8.56. Calc. for $C_{21}H_{27}N_3O_9$·1.2H2O: C, 52.18; H, 6.04; N, 8.70 %. HRMS-ESI+ (m/z) : [M+H]+ calcd for $C_{21}H_{27}N_3O_9Na$, 488.1645, found 488.1633. IR vmax (cm^{-1}): 3366s, 2967w, 1722s, 1707s, 1635s, 1556w, 1531s, 1477m, 1407m, 1339m, 1288s, 1261m, 1177s, 1094m, 936m, 857m, 736w, 720m, 605w, 578w.

Trimethyl 5, 5', 5''-((benzene-1,3,5- tri(carboxamide)) tris pentanoic acid 3: Yield 77%; mp 158 ˚C. 1H NMR (DMSO-d6, 600 MHz, δ) 12.01 (s, 3H, OH), 8.67 (t, J = 5.1 Hz, 3H, NH), 8.36 (s, 3H, Aromatic), 3.29 (overlapping with H2O signal), 2.25 (apparent s, 6H, 4-CH2), 1.55 (apparent s, 12H, 2-CH2,3-CH2). 13C NMR (DMSO-d6, 150 Hz, δ) 174.9 (COOH), 165.9 (CONH), 135.6 (Aromatic), 128.8 (C5), 33.8 (4), 29 (C1), 22.5 (C2, C3). Found: C, 55.81; H, 6.63; N, 8.13. Calc. for $C_{24}H_{33}N_3O_9$·0.4 H_2O·0.25 CH_3OH: C, 55.80; H, 6.64; N, 8.14 %. HRMS-ESI+ (m/z): [M+H]+ calcd. for $C_{24}H_{34}N_3O_9$, 508.2295, found 508.2286. IR vmax (cm-1): 3345m, 2929m, 1711s, 1612s, 1588m, 1541s, 1460m, 1428w, 1411w, 1311w, 1299m, 1269w,

1241m, 1220w, 1186s, 1101w, 1069w, 1034w, 928m, 915m, 839w, 777w, 747m, 693m, 640m, 566w.

Trimethyl 6, 6', 6''-((benzene-1,3,5- tri(carboxamide)) tris hexanoic acid 5: Yield 94%; mp 144 ˚C. ^{1}H NMR (DMSO-d_6, 600 MHz, δ) 11.98 (s, 3H, OH), 8.65 (t, 3H, 5.5 Hz, NH), 8.36 (s, 3H, Aromatic), 3.27 (overlapping with H_2O signal, 6H, 1-CH2), 2.21 (t, 6H, 7.4 Hz, 5-CH2), 1.54 (m, 12 H, 2-CH2, 4-CH2), 1.32 (m, 6H, 3-CH2). ^{13}C NMR (DMSO-d_6, 150 Hz, δ) 174.43 (COOH), 165.4 (CONH), 135.1 (Aromatic), 128.27 (C6), 33.59 (C5), 28.75 (C1), 26.0 (C2, C4), 24.2 (C3). Found: C, 57.89; H, 7.22; N, 7.38. Calc. for $C_{27}H_{39}N_3O_9 \cdot 0.66\ H_2O$: C, 57.76; H, 7.24; N, 7.48 %. HRMS-ESI$^-$ (*m/z*) : [M-H]$^-$ calcd for $C_{27}H_{38}N_3O_9$, 548.2608, found 548.2599. IR ν_{max} (cm^{-1}): 3364m, 3317w, 2946m, 1697s, 1636s, 1587w, 1540m, 1461w, 1410m, 1342w, 1273s, 1236m, 1187s, 1107m, 1064w, 874w, 789w, 715w, 654m, 611w, 580w.

Results and Discussion

Synthesis and Structural Studies

The ester derivatives **2** and **4** were prepared in good yields using the established protocols for symmetric tri-substitution of benzene-1,3,5-tricarbonyl trichloride, using ester-protected amino acids of various chain lengths (Scheme 1). These compounds, as well as the previously reported ester derivative of **1**, **Me$_3$-1**,[6] could be converted to the corresponding carboxylic acids by base hydrolysis followed by acidification to precipitate the neutral compounds in good to quantitiative yields. Long, needle-like crystals of **1-4** were obtained by slow evaporation of varying solvents (2:1 H_2O/THF, H_2O, 1:1 H_2O/CH_3OH, 2:1 H_2O/THF, respectively).‡ However, despite repeated attempts, single crystals of suitable quality could not be obtained for **5**.

Structure of 1

A crystal of **1** was subjected to X-ray diffraction and the data obtained were solved and the structure model refined in the triclinic space group *P*-1. The asymmetric unit is shown in Figure 1.

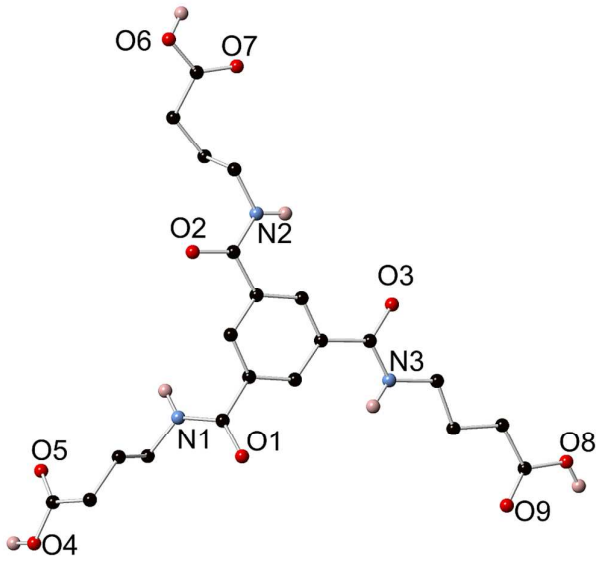

Figure 1 Structure of compound **1** with heteroatom labelling scheme. Selected hydrogen atoms are omitted for clarity.

The entire molecule is present within the asymmetric unit, and each of the three unique aliphatic arms exhibits a slightly different conformation. One arm, containing amide group C7, O1 and N1, displays a slightly twisted configuration with respect to the central ring (amide – ring interplanar angle 26.9°), compared to the other two unique amides which are effectively coplanar with the central phenyl ring. Additionally, one of the three aliphatic arms, originating from amide group C17, O3 and N3, exhibits fully staggered dihedral angles resulting in an overall linear arrangement, while the remaining two arms both contain a combination of staggered and *gauche* conformations resulting in non-equivalent, twisted arrangements.

Intermolecular interactions within the structure of **1** predominantly involve hydrogen bonding interactions, with the molecule containing six non-equivalent hydrogen bond donors and six possible acceptors, as depicted in Figure 2 (top). Nonetheless, the resulting hydrogen-bonded network is remarkably symmetric in nature. Each of the three unique arms interacts with its symmetry equivalent to generate four hydrogen bonds per pairing, Figure 2 (top). In each case, three edge-sharing hydrogen-bonded rings are formed. Two $R_2^2(12)$ rings are present, defined by O-H···O interactions between carboxylic acid groups and amide oxygen atoms and N-H···O

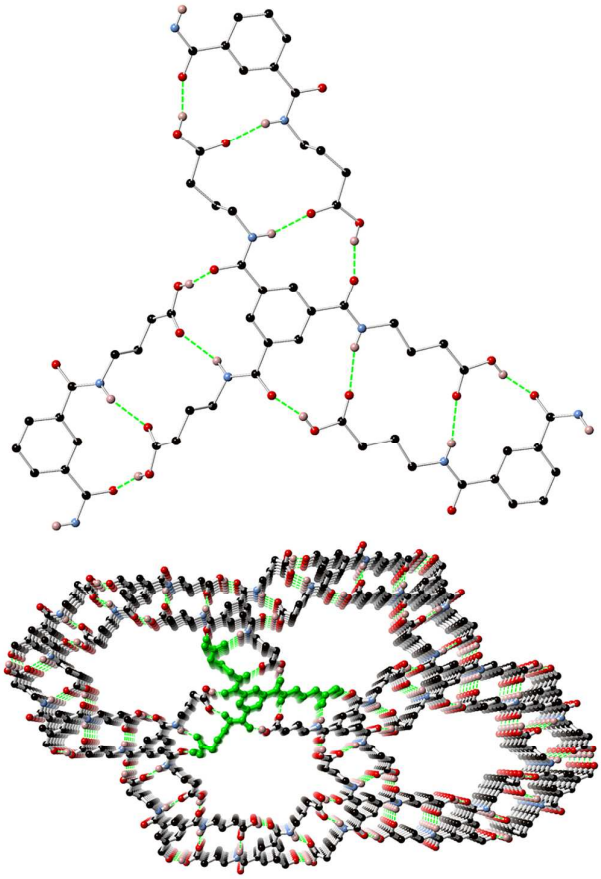

Figure 2 (Top) Hydrogen bonding interactions between adjacent molecules in the structure of **1**. Hydrogen atoms not involved in hydrogen bonding interactions are omitted for clarity. (Bottom) Extended structure of **1** viewed parallel to the solvent channels.

interactions between amide N-H groups and carboxylate oxygen atoms. These rings are linked by edge-sharing with a central centrosymmetric $R_2^2(14)$ loop containing the N-H··O interactions, as depicted in Figure 2 (bottom).

By virtue of the hydrogen bonding interactions, each molecule of **1** interacts with three others, to form an extended 2-dimensional (6,3) hydrogen bonded network. Adjacent layers of this network associate by π-π type interactions, with overlap of π systems taking place between the phenyl rings and amide groups from adjacent layers at minimum (interatomic) distance of 3.352(4) Å for C1-C12. This packing arrangement leaves one-dimensional hexagonal channels parallel to the crystallographic *a* axis, of approximately 10 Å (interatomic) diameter. The contents of these channels could not be sensibly modelled from the crystallographic data due to poor ordering of the guest molecules, presumably related to the lack of strongly interacting groups (hydrogen bond donors or otherwise) directed into the channels. As such, the contribution from the disordered guest molecules to the measured structure factors was accounted for using the SQUEEZE routine in PLATON,[24] and the exact content of the solvent channels was determined by elemental analysis.

Elemental analysis revealed the presence of 1.2 H_2O molecules per molecule of **1** for an air-dried sample. The freshly isolated compound **1**, however, showed a loss of ca. 39% mass below 100 °C by TGA, before decomposition with onset of approximately 250 °C (ESI). This analysis suggests greater occupancy of the solvent channels immediately after removal from solution, with the additional guest molecules gradually lost or exchanged for atmospheric water. The X-ray powder diffraction analysis of compound **1** showed that the phase identified from single crystal analysis was predominant in the bulk sample, which was unchanged on standing in air. A sample of **1** was subjected to exhaustive evacuation by heating at 100.0 °C under dynamic vacuum overnight, followed by testing for N_2 uptake at 77 K and CO_2 adsorption at 273 K. In both cases, however, negligible uptake was observed, suggesting a collapse of the framework upon complete desolvation.

Structure of 2

A crystal of **2** was subjected to single crystal X-ray diffraction, and the most sensible solution was obtained in the hexagonal space group $P6_3/m$, with a unit cell $a = b = 15.57$ Å, $c = 6.87$ Å (Table 1). The resulting structural model of **2** is represented in Figure 3. The substantial disorder encountered in **2** (Supporting Information) prompted an exhaustive search for larger unit cells and lower symmetry space groups. Although a related hexagonal cell with $a = b = 31.14$ Å could be indexed and solved in $P6_3$, equivalent disorder of the alkyl chains was encountered, with the added complication of a considerable loss of data quality based on the low intensity of the additional interstitial reflections, and related large correlation elements when refining U_{ij} tensors for pseudo-symmetry-related atom sites. Equivalent disorder was also encountered in all lower symmetry space groups examined, including *P*1. As such, the structure model is presented as the best available description from the crystallographic data, allowing the presence of an *m* symmetry element coincident to the phenyl ring plane to suitably model the disordered chain orientations between adjacent stacks without introducing redundant additional parameters in a lower symmetry space group.

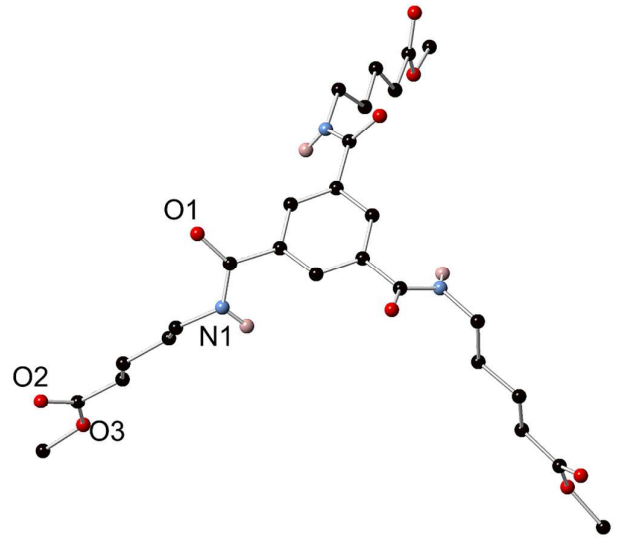

Figure 3 Structure of **2** with labelling scheme for unique heteroatoms. Selected hydrogen atoms and crystallographic disorder are omitted for clarity.

As modelled, the asymmetric unit of **2** contains one-third of the molecule, with a crystallographic threefold rotation axis coincident with the centre of the phenyl ring. The alkyl chains are modelled as disordered over two orientations, originating from two possible symmetry-related orientations of the amide groups from which the aliphatic chains extend in a linear fashion. The extended structure of **2** consists of one-dimensional hydrogen-bonded stacks of aromatic groups, with each pair supported by three equivalent N-H···O hydrogen bonding interactions (N···O distance 2.825(4) Å, angle N-H···O 159(4)°), Figure 4 (top). Adjacent phenyl rings are separated by an interplanar or minimum interatomic distance of 3.4134(3) Å, half the length of the crystallographic *c* axis. Although the disorder inherent in the phenyl-amide torsion angle obscures the precise nature of the extended hydrogen bonding network, a triple-helical arrangement of hydrogen bonding interactions around the central column is most likely, based on precedence in similar compounds[6, 25] and the unfavourable geometric mismatch which would occur in the case of a statistical mixture of orientations within a single stack. Adjacent columns align in a hexagonal close packed manner with the disordered aliphatic chains interdigitated in the interstitial spaces. No solvent or guest molecules were detected within the structure, nor were the presence of any additional species indicated by elemental analysis. X-ray powder diffraction of the bulk material showed no obvious evidence of other polymorphs at room temperature (Supporting Information).

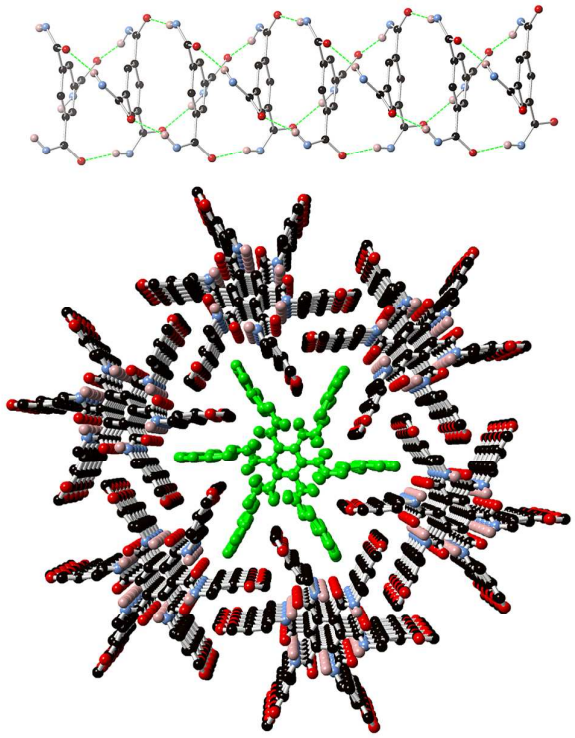

Figure 4 (Top) Representation of the helical hydrogen bonding motif present within columns in the structure of 2. C-H hydrogen atoms, crystallographic disorder of amide groups, and alkyl arms are omitted for clarity. (Bottom) Extended structure of **2** showing hexagonal close packing of adjacent columns, with single column highlighted in green.

Structure of 3

A crystal of **3** was analysed by single crystal X-ray diffraction, and the data were solved and refined in the monoclinic space group *P*2/*n*, Figure 5. The asymmetric unit contains the entire molecule, as well as five unique and well-localised water molecules. Each of the three amido-carboxylic acid arms is crystallographically non-equivalent, and each adopts a folded conformation. One of the three amide groups displays a significant torsion to the phenyl ring mean plane (interplanar angle 29.8°), while the remaining two amide groups are essentially coplanar with the ring, Figure 5.

The extended structure of **3** contains myriad hydrogen bonding interactions both between **3** molecules and involving the lattice water molecules. Three unique motifs are observed when analysing the hydrogen bonding interactions in **3**. One of the three amido acid arms, originating from amide nitrogen atom N3, undergoes a reciprocated interaction with a symmetry-equivalent arm involving two $R_2^2(12)$ rings edge-shared with an $R_2^2(16)$ motif. This pattern is equivalent to that observed in the structure of **1** while allowing for the increase in chain length, in which each carboxylic acid group donates one hydrogen bond to an amide oxygen atom and accepts one hydrogen bond from the N-H site of a different amide group on the same molecule. The amido-acid arm originating from nitrogen atom N2 is involved in a similar interaction, which shares the central $R_2^2(16)$ motif. However, the terminal

carboxylic acid groups are arranged in a divergent manner, in which the O-H···O interaction originating from oxygen atom O6 is directed at a different molecule than the N-H···O contact which is received from nitrogen atom N2. The two remaining hydrogen bond donors in the molecule, N1 and O3, both donate hydrogen bonds to lattice water molecules.

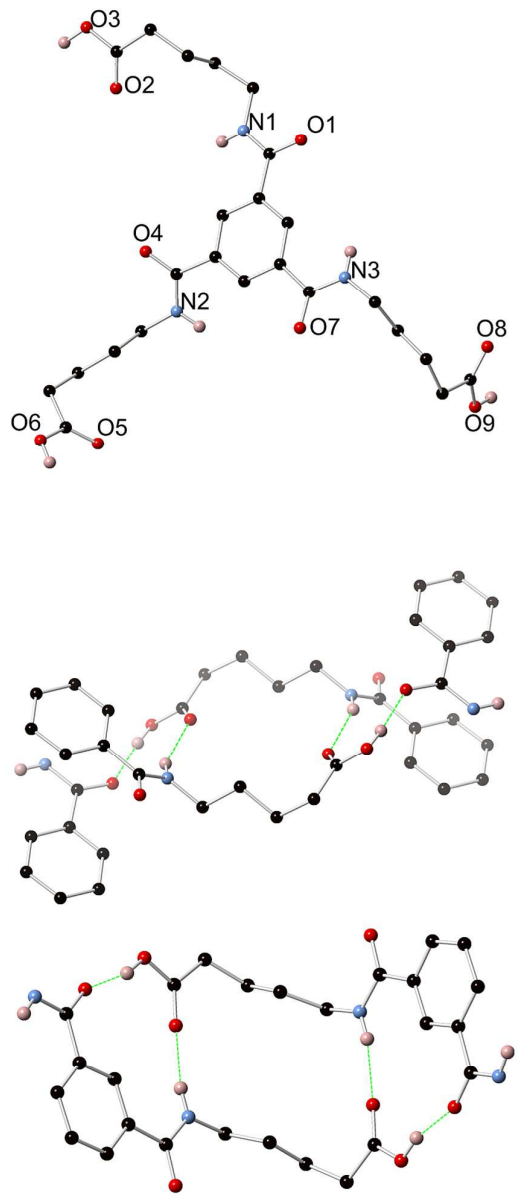

Figure 5 (Top) Structure of **3** with heteroatom labelling scheme. Selected hydrogen atoms and crystallographic disorder are omitted for clarity. (Bottom) The two unique modes of intermolecular hydrogen bonding present in the structure of **3**.

The linkages through hydrogen bonding interactions and minor amide-phenyl π-π interactions propagate a 3-dimensional assembly in the structure of **3**, leaving one-dimensional channels parallel to the crystallographic b axis centered on a twofold axis of symmetry, with an approximate (interatomic) diameter of 8.5 Å, Figure 6. Within this channel resides a one-dimensional hydrogen-bonded water cluster with a repeating unit of five unique water molecules. The approximate orientations for the hydrogen atoms associated

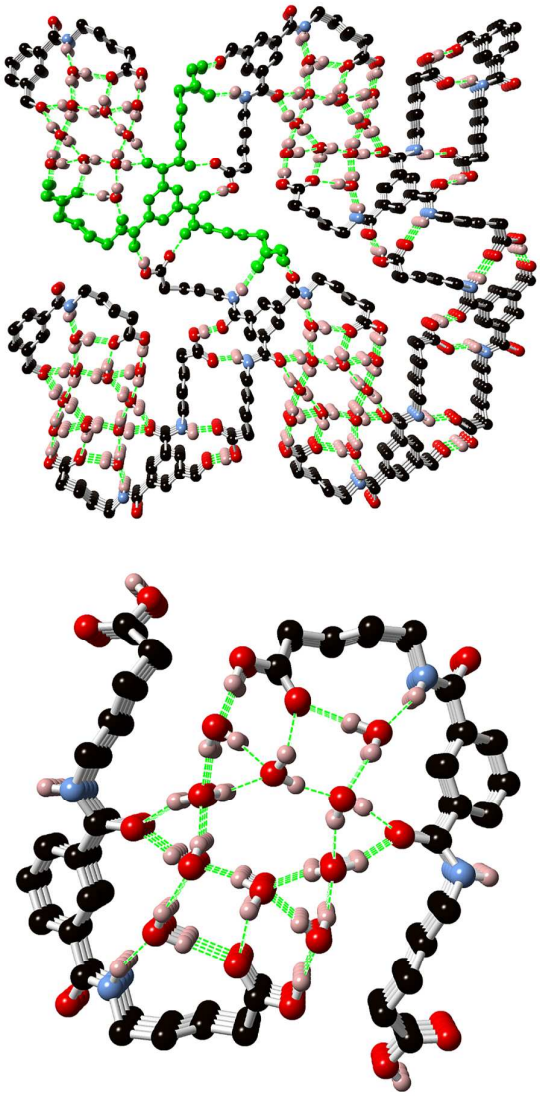

Figure 6 (Top) Extended structure of **3** showing linkages through adjacent stacks of molecules via polymeric water clusters. A single molecule of **3** is highlighted in green. (Bottom) A single columnar water cluster in the structure of **3** with bordering organic groups. Selected hydrogen atoms are omitted for clarity.

with these water molecules could be deduced from the locations of the Fourier residuals, and the atom positions were allowed to freely refine with loose H-O distance restraints and riding U_{iso} dependencies. The five water molecules cumulatively accept eight hydrogen bonds; water molecules O12 and O14 accept one hydrogen bond each from framework atoms N1 (amide) and O3 (carboxylic acid), respectively, and the remaining three water molecules accept six hydrogen bonds originating from other and symmetry-related water molecules. Framework atoms O2 (carboxylic acid) and O4

(amide) each accept two hydrogen bonds from lattice water molecules.

A freshly isolated sample of compound **3** showed a loss of 25 wt % before 80 °C by TGA, corresponding to the loss of both surface water and water present in the channels. TGA measurements on a vacuum-dried sample revealed no mass loss until decomposition began at approximately 200 °C (ESI). Time course X-ray powder diffraction studies of the crystalline material showed that the peaks due to the original crystalline phase begun to disappear almost immediately on removal from solvent, and are replaced by new peaks corresponding to a second, unidentified crystalline phase coinciding with the disturbance of the lattice solvent. Despite our efforts, we were unable to collect meaningful single-crystal data on this poorly crystalline desolvated phase. Attempts to directly re-solvate the collapsed material with water led to immediate loss of crystallinity, indicating the first phase transition is irreversible.

Although examples of permanent porosity are rare in hydrogen-bonded molecular crystals, stability to evacuation can be conferred in instances where the pore architectures are supported by multiple strong hydrogen bonding interactions.[26] A sample of **3** was thoroughly dried under dynamic vacuum at 100.0 °C and the resulting compressed material examined for gas adsorption behaviour. However, both the 77 K N_2 and 273 K CO_2 uptake experiments failed to provide any meaningful adsorption above the instrumental detection limit. These measurements would suggest that compound **3** immediately transitions to a collapsed, non-porous crystalline phase upon desolvation.

Structure of 4

A crystal of **4** was analysed by single crystal X-ray diffraction, and the data were solved and refined in the monoclinic space group $P2_1/c$. The asymmetric unit contains the molecule in its entirety, Figure 7, with no associated solvent or guest molecules.

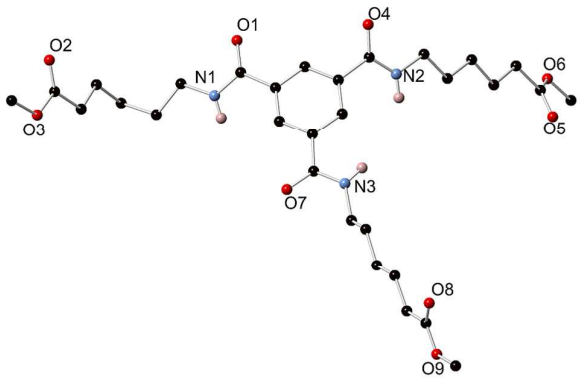

Figure 7 Structure of **4** with heteroatom labelling scheme. Selected hydrogen atoms and crystallographic disorder are omitted for clarity.

Similarly to the case of **1**, each of the three aliphatic arms adopts a slightly different conformation in **4**. The three amide groups display varying degrees of planarity with the central phenyl ring, with amide-phenyl mean interplanar angles 21.6°, 7.6° and 39.4° for the three amides defined by N1/O1, N2/O2 and N3/O3 respectively. These distortions represent both twisting about the C(amide)-C(phenyl) bonds, related to the three associated dihedral angles of 19.0(8)°, 8.5(8)° and 36.7(6)° respectively, and folding of the amide group out of the phenyl ring plane. Two of the three aliphatic chains adopt linear fully staggered conformations, while the other, originating from amide nitrogen atom N1, contains *gauche* conformers at methylene groups C13 and C14 leading to a bent arrangement for the chain.

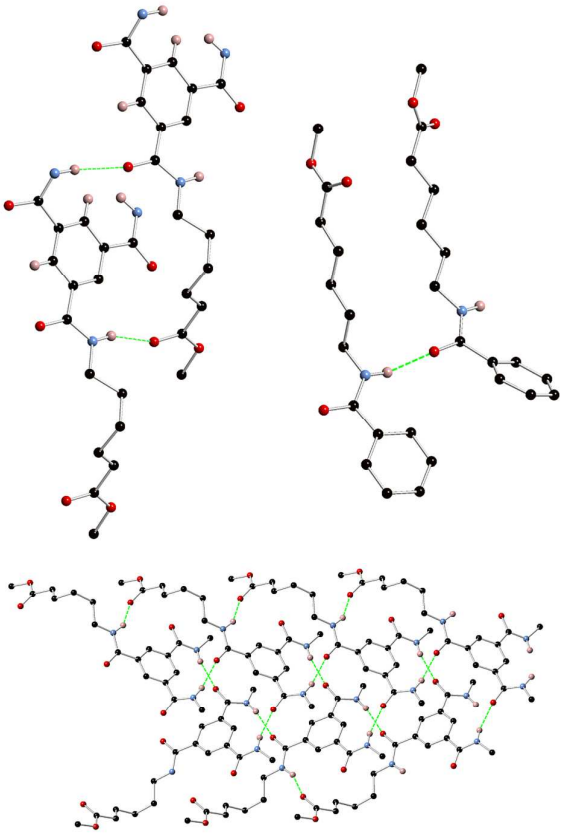

Figure 8 (Top) The unusual $R_2^2(19)$ loop interaction of the amide donors of **4**. (Bottom) Extended structure of **4** showing the densely packed structure.

Intermolecular interactions in the structure of **4** consist primarily of hydrogen bonds originating from the amide N-H groups, interacting with carbonyl oxygen atoms from adjacent amide or ester functional groups. The aliphatic chain originating from amide nitrogen atom N1 engages in two hydrogen bonding interactions with the same adjacent molecule, acting as a hydrogen bond acceptor at both amide and ester oxygen atoms O1 and O2, from two amide nitrogen atoms N1 and N2. This interaction can be considered as an unusual $R_2^2(19)$ loop which spans two amide donors across the width of the central phenyl ring, and is accommodated by the bent arrangement of the doubly-accepting amido-ester chain, Figure 8. The remaining amide nitrogen atom N3 participates in an N-H··O hydrogen bonding interaction with amide oxygen

atom O4. Slight positional disorder was encountered on the two ester moieties not engaging in hydrogen bonding interactions, and these groups were modelled, after free variable refinement to determine the occupancy of the disordered contributors, split at 0.75:0.25 and 0.85:0.15 occupancy for O8/O9 and O5/O6, respectively. The hydrogen bonding between molecules of **4** propagates a densely packed network, and no void space was detected within the structure. Although elemental analysis of **4** confirmed the bulk formulation to match that observed in the crystal structure, X-ray powder diffraction revealed the presence of a mixture of polymorphs; we were unable to characterise the additional phases by single crystal X-ray diffraction, nor could the phases be separated or selectively prepared synthetically, though the relative distributions of the polymorphic phases could be influenced by thermal cycling of the as-synthesised material, and indicated that at least one component of the mixed phase system bears a strong resemblance to the columnar phase **2** (Supporting information). The phase behaviour of **4** was further probed using Differential Scanning Calorimetry (DSC), as described below.

Thermal Analysis

Inspired by previous reports,[17, 27] and the discotic columnar packing motif present in the structure of **2**, the existence of additional high-temperature crystalline phases or thermotropic mesophases of **1** – **5** was investigated (Table 2) using differential scanning calorimetry (DSC) and polarised optical microscopy (POM). Although the synthesis and characterisation of the methyl ester precursor to **1**, **1-Me$_3$** has been previously reported,[6] no thermal studies have been previously carried out. As such, this material was also subjected to analysis by DSC to provide a short-chain baseline measurement. In each of the three temperature cycles, **1-Me$_3$** showed only Cr-I and I-Cr transitions on the heating and cooling cycles, respectively, with no evidence of any additional phases (See ESI). Additionally, all three of the carboxylic acid derivatives **1**, **3** and **5** were subjected to analysis by DSC. Each showed a well-resolved melting transition on the first heating cycle, as well as the loss of encapsulated solvent, followed by freezing into amorphous phases on cooling which presented no obvious distinct phase transitions on additional heating and cooling cycles (ESI).

DSC measurements of **2** revealed a single endothermic transition on the heating cycle, the melting (Cr-I) transition onset at 81.6 °C, with Δ_H = 39.7 kJ/mol, corresponding to the observed melting point of 89-90 °C, Table 2. Two exothermic transitions were observed on the cooling cycle, a lower energy exothermic step with an onset temperature of 71.5 °C followed by a more substantial exotherm at 60.6 °C. These transitions show Δ_H values of -5.2 kJ/mol and -35.3 kJ/mol respectively, and along with the melting transition are reproducible over multiple heating and cooling cycles. The material was examined under polarised light at temperatures corresponding to each of the observed phases, on both heating and cooling steps. On cooling from the isotropic melt, birefringent texture is observed following the first exothermic transition, characteristic of an ordered phase. Further cooling led to roughening of the droplets and re-generation of the original crystalline phase, evidenced by X-ray powder diffraction at room temperature (ESI).

Similarly, compound **4** was subjected to investigation by DSC and POM. DSC analysis revealed endothermic transition onsets at 59.3 °C, 75.1°C and 95.5 °C, with transition enthalpies of 9.4, 8.9 and 5.9 kJ/mol respectively. On the cooling cycle, exothermic transition onsets were observed at 98.6 °C and 57.2 °C, with transition enthalpies of -6.1 and -11.8 kJ/mol. We ascribe the first endothermic transition, with a broad exothermic tail, to a recrystallization process, converting the Cr1 low-temperature crystalline phase to a high-temperature crystalline phase. X-ray powder diffraction of this material (ESI) after heating to 75.0 °C in air showed marked differences in the positions and intensity of the major Bragg peaks compared to the pristine sample, itself most likely a mixture of polymorphic phases. On successive heating cycles in the range 30.0 – 74.0 °C, the major endothermic peak centred at 63.0 °C diminished, indicating eventual conversion to the high temperature crystalline phase without re-formation of the low temperature phase on cooling (ESI). The phase transition temperatures agreed closely with the data obtained by POM, as seen in supporting information.

Compound	Heating cycle onset temperature (ΔH)	Cooling cycle onset temperature (ΔH)
2	81.6 °C (39.73kJ/mol)	71.5 °C (-5.2 kJ/mol) 60.6 °C (-35.3 kJ/mol)
4	59.3 °C (9.4 kJ/mol) 64.1 °C (-6.2 kJ/mol) 75.1 °C (8.9 kJ/mol) 94.5 °C (5.9 kJ/mol)	98.6 °C (-6.1 kJ/mol) 57.2 °C (-11.8 kJ/mol)

Table 2 Summary table of onset temperatures for endo- and exothermic transitions for compounds **2** and **4**.

Gelation studies

The propensity for **BTA** derivatives to form organogels has been widely reported.[8, 12] Given the fibrous nature of the crystals formed by each of the compounds, the gelation abilities of **1-5** in a variety of solvent conditions were also investigated. Gel formation was not observed under any conditions investigated for the ester derivatives **2** and **4**, which generally formed crystalline or micro-crystalline solids upon precipitation.

After screening experiments in a wide range of common solvents, gelation of the carboxylic acid derivatives was found to be most effective by dissolving the appropriate compound at 1 wt % in 2:1 H_2O:THF mixtures with gentle heating, and allowing the mixtures to set over several days. Compound **5** readily forms a gel under these conditions, while **1** forms a very weak gel (ESI). We were unable to reliably generate gels from compound **3** under the same conditions, although gelation could be induced in small quantities of solvent by this method. It was not possible to reproducibly scale the preparation to useful quantities, nor could gelation be induced

in different solvent mixtures or concentrations. Visually, and using the well-established 'inversion test',[28] the compound **5** gel appeared robust, and maintained resistance to inversion at 2.4 % wt, confirmed by thermogravimetric analysis. The lowest % wt obtained for **3** was 2.5 % wt (by TGA). In contrast, compound **1** formed only weak gels and required higher solid loadings to achieve a gel phase (5.0 % wt by TGA). These observations would corroborate the intuitive expectation that the length of the aliphatic chain influences the strength of the gel network formed.

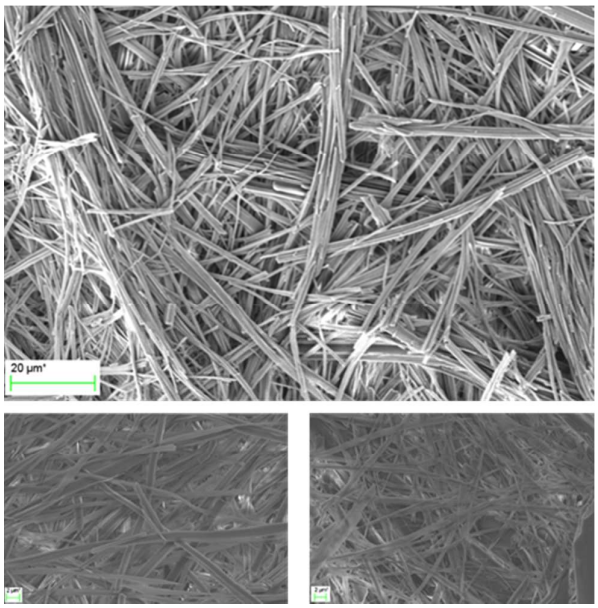

Figure 9 SEM of xerogels of **5** (top), **3** (bottom left, scale bar 2 µm) and **1** (bottom right, scale bar 2 µm), revealing their fibrous morphology.

The morphology of the xerogels obtained by drying the **1**, **3** and **5** (H_2O/THF) gels under dynamic vacuum was examined by Scanning Electron Microscopy (SEM), as shown in Figure 9. These images reveal the entangled fibrous nature of the materials and consistently show fibres with a diameter of approximately 500 nm. The fibrous nature of the gels is also visible in the bulk scale under optical magnification (ESI).

The robust and reproducible gel formed from **5** prompted further, quantitative rheological studies to be carried out on this material. On compression in the sample chamber of the rheometer, however, phase separation was observed, resulting in a contraction of the gel matrix and liberation of a portion of the encapsulated liquid solvent. To generate a robust and homogenous gel material for the bulk measurement, the original 2.4 % wt gel was compressed until separation of the solvent was no longer observed. This sample preparation resulted in an approximate tenfold increase in the solid fraction, with the material undergoing loss of 75% weight below 86 °C by TGA (ESI).

To gain an understanding of the mechanical properties of the gel materials, rheological studies were carried out. Focusing on ligand **5**, strain and frequency sweeps and a recovery test on the compressed gel of **5** were carried out, and the results of the strain experiments are shown in Figure 10. The storage modulus G' initially takes a value of 3.12×10^6 Pa, an order of magnitude greater than the loss modulus G'' at the same strain amplitude, as is expected for a solid-like material, with a crossover occurring at the yield strain 0.78 % indicating a change to a liquid-like phase. The frequency sweep experiment demonstrates that the elastic response in the linear viscoelastic regime is insensitive to frequency. The recovery properties of **5** were investigated with an oscillatory recovery test, showing the effect on the storage and loss moduli at low strain amplitude in the linear viscoelastic regime after shearing far beyond the yield point with the results shown in Figure 10. This experiment shows that the gel **5** rapidly returns to its original strength after shearing, and this behaviour is maintained over repeated cycles.

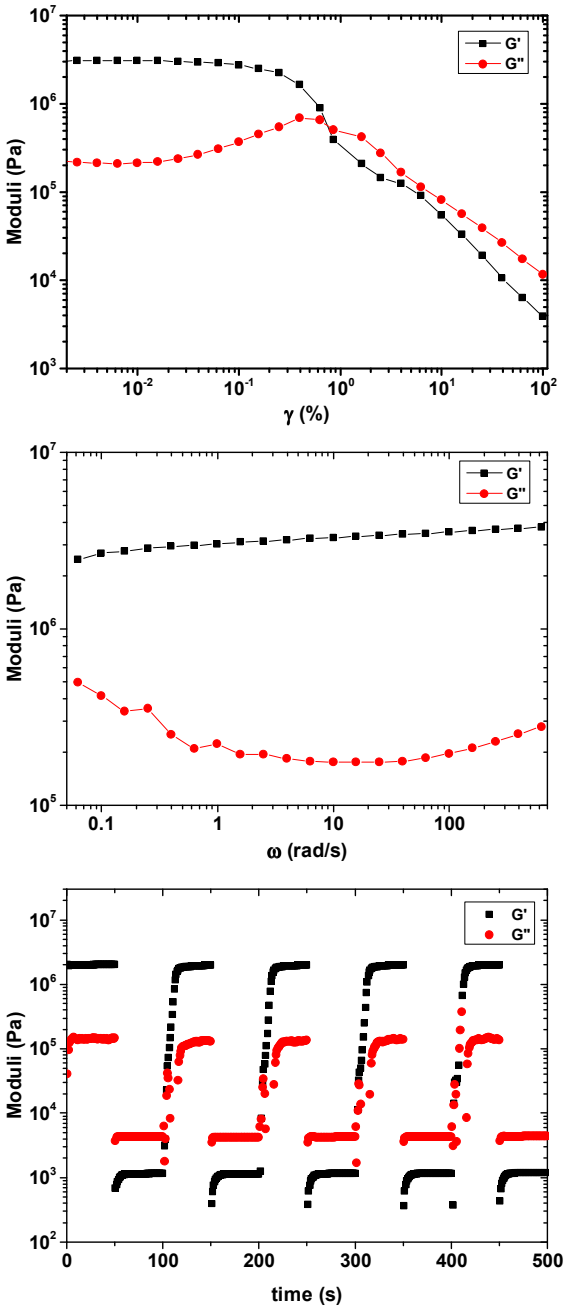

Figure 10 Strain sweep experiment showing the crossover from solid to liquid-like behaviour (top) at $\omega = 6.28$ rad/s, frequency sweep experiment (middle) at $\gamma = 0.01\%$ and recovery test (bottom), demonstrating the mechanical reversibility of the gel. Here, the strain amplitude was alternating between $\gamma = 0.01\%$ (solid-like) and $\gamma = 500\%$ (liquid-like) for 50 seconds each over 5 cycles at $\omega = 6.28$ rad/s.

Discussion

The structural, rheological and thermal behaviours of compounds **1** – **5** and **1-Me$_3$** show the effect of functional group and chain length variation on self-assembly behaviour of these **BTA** derivatives. It is clear that gelation of these systems requires the additional strong intermolecular interactions provided by the carboxylic acid groups, a property which is not observed in the weakly interacting ester derivatives. However, the presence of these strongly interacting groups serves to both raise the melting points of the acid derivatives and leads to strongly interconnected network structures, both of which tend towards irreversible crystalline-amorphous transitions on melting. In contrast, the ester derivatives **2** and **4** each display one-dimensional hydrogen bonded superstructures in the crystalline phase, with only weak interactions between strands, particularly in the case of the poorly ordered columnar phase **2**. The tendency for weak interactions between adjacently aligned one-dimensional columnar architectures is consistent with the observed thermal behaviour of compounds **2** and **4,** is a pre-requisite for, for example, columnar discotic liquid crystal behaviour.

Besides the clear variation in bulk properties between the ester and carboxylic acid compounds, more subtle variations were observed within each class as a function of chain length. As expected, the shortest chain compounds **1** and **1-Me$_3$** showed the greatest tendency towards crystallinity in each of the phases studied; the ester **1-Me$_3$** showed only discrete melting and crystallisation transitions under thermal analysis, and the acid derivative **1** formed weak gels consisting largely of crystalline fibres. The prevalence of additional thermotropic phases for the ester derivatives and the gel materials for the acid derivatives subsequently improved with increasing chain length. Interestingly, extension of the alkyl chain by one carbon atom between **2** and **4** led to a transition in the crystalline phase from the well-known helical **BTA** stacking motif to a disrupted packing motif containing an $R_2^2(19)$ loop across the breadth of the aromatic core. However, the presence of two distinct crystalline phases in the thermal profile of **4** suggests that this low-temperature phase may represent a kinetic product. The chain length dependences of the carboxylic acid derivatives were largely manifested in variations in the tendency to form robust gel materials, which increased with chain length alongside a reduced tendency for single crystal formation. Although the additional hydrogen bonding capabilities led to the formation of two solvent-containing crystalline materials, neither material showed stability to evacuation. This is most likely due to the high degree of backbone flexibility in each material, a common source of structural weakness in crystalline organic assemblies and flexible metal-organic frameworks alike.[29]

Conclusions

We have prepared five carboxylic acid or carboxymethyl derivatives of benzene-1,3,5-tricarboxamide with alkyl chains of various lengths, and studied the structural and physical properties of the resulting materials. The carboxylic acid derivatives **1** and **3** formed crystalline materials containing well-resolved solvent channels, which were destroyed upon drying in air or under dynamic vacuum. However, **5**, bearing the longest carboxylic acid chain, formed a robust and reproducible gel from a H_2O/THF mixture. This gel displays the expected fibrous morphology under SEM, and displays thixotropic behaviour on shearing.

In contrast to these results, the ester derivatives **2** and **4** both exhibited multiple phase changes on heating and cooling cycles, consistent with their weakly associated columnar packing behaviour in the crystalline state. These findings provide further scope in the development of responsive soft materials based on **BTA**-derived molecules, where the balance of the intrinsic aggregation properties of the core can be offset by subtle variations in substitution patterns; this approach is currently being further pursued in our laboratory.

Acknowledgements

The authors gratefully acknowledge the Irish Research Council (IRC) for (Postdoctoral Fellowship GOIPD/2015/446 to CSH), Science Foundation Ireland (SFI) for SFI PI Awards (10/IN.1/B2999 and 13/IA/1865 to TG, 13/IA/1896 to WS, 13/IA/1926 to MM), MPNS COST Actions MP1106 and MP1305, ESA (A0-99-075 and contract 4000115113), TCD Dean of Research Pathfinder Award (TG and CSH), the European Research Council (ERC; CoG 2014 – 647719 to WS), TCD School of Chemistry and Royal Society URF for financial support.

Notes and references

‡ CCDC 1503992-1503995.

1. T. R. Canrinus, F. J. R. Cerpentier, B. L. Feringa and W. R. Browne, *Chem. Commun.*, 2017, DOI: 10.1039/C7CC00017K; K. W. K. Tong, S. Dehn, J. E. A. Webb, K. Nakamura, F. Braet and P. Thordarson, *Langmuir*, 2009, **25**, 8586-8592; O. Kotova, R. Daly, C. M. G. dos Santos, P. E. Kruger, J. J. Boland and T. Gunnlaugsson, *Inorg. Chem.*, 2015, **54**, 7735-7741; R. Daly, O. Kotova, M. Boese, T. Gunnlaugsson and J. J. Boland, *ACS Nano*, 2013, **7**, 4838-4845.
2. T. Gunnlaugsson, *Nat Chem*, 2016, **8**, 6-7; E. P. McCarney, J. P. Byrne, B. Twamley, M. Martinez-Calvo, G. Ryan, M. E. Mobius and T. Gunnlaugsson, *Chem. Commun.*, 2015, **51**, 14123-14126; S. J. Bradberry, A. J. Savyasachi, R. D. Peacock and T. Gunnlaugsson, *Faraday Discuss.*, 2015, **185**, 413-431; M. Martínez-Calvo, O. Kotova, M. E. Möbius, A. P. Bell, T. McCabe, J. J. Boland and T. Gunnlaugsson, *J. Am. Chem. Soc.*, 2015, **137**, 1983-1992; J. P. Byrne, J. A. Kitchen and T. Gunnlaugsson, *Chem. Soc. Rev.*, 2014, **43**, 5302-5325; J. P. Byrne, J. A. Kitchen, O. Kotova, V. Leigh, A. P. Bell, J. J. Boland, M. Albrecht and T. Gunnlaugsson, *Dalton Trans.*, 2014, **43**, 196-209; M. de Loos, J. H. van Esch, R. M. Kellogg and B. L. Feringa, *Tetrahedron*, 2007, **63**, 7285-7301.
3. S. Cantekin, T. F. A. de Greef and A. R. A. Palmans, *Chem. Soc. Rev.*, 2012, **41**, 6125-6137.
4. P. J. M. Stals, J. C. Everts, R. de Bruijn, I. A. W. Filot, M. M. J. Smulders, R. Martín-Rapún, E. A. Pidko, T. F. A. de Greef, A. R. A. Palmans and E. W. Meijer, *Chem. Eur. J.*, 2010, **16**, 810-821.
5. P. Jana, A. Paikar, S. Bera, S. K. Maity and D. Haldar, *Org. Lett.*, 2014, **16**, 38-41.
6. A. Paikar, A. Pramanik and D. Haldar, *RSC Adv.*, 2015, **5**, 31845-31851.
7. P. Besenius, G. Portale, P. H. H. Bomans, H. M. Janssen, A. R. A. Palmans and E. W. Meijer, *Proc. Natl. Acad. Sci. U.S.A.*, 2010, **107**, 17888-17893.
8. R. C. T. Howe, A. P. Smalley, A. P. M. Guttenplan, M. W. R. Doggett, M. D. Eddleston, J. C. Tan and G. O. Lloyd, *Chem. Commun.*, 2013, **49**, 4268-4270.
9. A. Desmarchelier, M. Raynal, P. Brocorens, N. Vanthuyne and L. Bouteiller, *Chem. Commun.*, 2015, **51**, 7397-7400; P. J. M. Stals, P. A. Korevaar, M. A. J. Gillissen, T. F. A. de Greef, C. F. C. Fitié, R. P. Sijbesma, A. R. A. Palmans and E. W. Meijer, *Angew. Chem. Int. Ed.*, 2012, **51**, 11297-11301; M. A. J. Veld, D. Haveman, A. R. A. Palmans and E. W. Meijer, *Soft Matter*, 2011, **7**, 524-531.
10. M. M. J. Smulders, P. J. M. Stals, T. Mes, T. F. E. Paffen, A. P. H. J. Schenning, A. R. A. Palmans and E. W. Meijer, *J. Am. Chem. Soc.*, 2010, **132**, 620-626; C. F. C. Fitié, I. Tomatsu, D. Byelov, W. H. de Jeu and R. P. Sijbesma, *Chem. Mater.*, 2008, **20**, 2394-2404.
11. A. Desmarchelier, B. G. Alvarenga, X. Caumes, L. Dubreucq, C. Troufflard, M. Tessier, N. Vanthuyne, J. Ide, T. Maistriaux, D. Beljonne, P. Brocorens, R. Lazzaroni, M. Raynal and L. Bouteiller, *Soft Matter*, 2016, **12**, 7824-7838.
12. O. Kotova, R. Daly, C. M. G. dos Santos, M. Boese, P. E. Kruger, J. J. Boland and T. Gunnlaugsson, *Angew. Chem. Int. Ed.*, 2012, **51**, 7208-7212.
13. C. M. G. dos Santos, E. M. Boyle, S. De Solis, P. E. Kruger and T. Gunnlaugsson, *Chem. Commun.*, 2011, **47**, 12176-12178.
14. K. Pandurangan, J. A. Kitchen, S. Blasco, E. M. Boyle, B. Fitzpatrick, M. Feeney, P. E. Kruger and T. Gunnlaugsson, *Angew. Chem. Int. Ed.*, 2015, **54**, 4566-4570.
15. Y. Matsunaga, N. Miyajima, Y. Nakayasu, S. Sakai and M. Yonenaga, *Bull. Chem. Soc. Jpn.*, 1988, **61**, 207-210; C. A. Jiménez, J. B. Belmar, L. Ortíz, P. Hidalgo, O. Fabelo, J. Pasán and C. Ruiz-Pérez, *Cryst. Growth Des.*, 2009, **9**, 4987-4989; C. M. A. Leenders, M. B. Baker, I. A. B. Pijpers, R. P. M. Lafleur, L. Albertazzi, A. R. A. Palmans and E. W. Meijer, *Soft Matter*, 2016, **12**, 2887-2893; C. M. A. Leenders, L. Albertazzi, T. Mes, M. M. E. Koenigs, A. R. A. Palmans and E. W. Meijer, *Chem. Commun.*, 2013, **49**, 1963-1965; M. M. J. Smulders, A. P. H. J. Schenning and E. W. Meijer, *J. Am. Chem. Soc.*, 2008, **130**, 606-611; M. Raynal, F. Portier, P. W. N. M. van Leeuwen and L. Bouteiller, *J. Am. Chem. Soc.*, 2013, **135**, 17687-17690.
16. P. J. M. Stals, J. F. Haveman, R. Martin-Rapun, C. F. C. Fitie, A. R. A. Palmans and E. W. Meijer, *J. Mater. Chem.*, 2009, **19**, 124-130.
17. C. F. C. Fitié, W. S. C. Roelofs, P. C. M. M. Magusin, M. Wübbenhorst, M. Kemerink and R. P. Sijbesma, *J. Phys. Chem. B*, 2012, **116**, 3928-3937.
18. P. J. M. Stals, M. M. J. Smulders, R. Martín-Rapún, A. R. A. Palmans and E. W. Meijer, *Chem. Eur. J.*, 2009, **15**, 2071-2080.
19. A. Bernet, R. Q. Albuquerque, M. Behr, S. T. Hoffmann and H.-W. Schmidt, *Soft Matter*, 2012, **8**, 66-69.
20. APEX-3, *Bruker-AXS Inc*, 2016, Madison, WI
21. SADABS, *Bruker-AXS Inc*, 2016, , Madison, WI.
22. G. M. Sheldrick, *Acta. Crystallogr. Sect A: Found Adv*, 2015, 3-8; G. M. Sheldrick, *Acta Crystallogr. Sect. C* 2015,

3-8; O. V. Dolomanov, Bouhis, L. J., Gildea, R. J., Howard, J. A. K., Puschmann, H. J., *Appl. Crystallogr.*, 2009, 339-341.

23. M. A. Ashraf, J. K. Notta and J. S. Snaith, *Tetrahedron Lett.*, 2003, **44**, 9115-9119.
24. A. L. Spek, *Acta Crystallogr Sect C.: Struct. Chem*, 2015, 9-18.
25. M. P. Lightfoot, F. S. Mair, R. G. Pritchard and J. E. Warren, *Chem. Commun.*, 1999, 1945-1946.
26. H. Wang, B. Li, H. Wu, T.-L. Hu, Z. Yao, W. Zhou, S. Xiang and B. Chen, *J. Am. Chem. Soc.*, 2015, **137**, 9963-9970.
27. A. R. A. Palmans, J. A. J. M. Vekemans, H. Fischer, R. A. Hikmet and E. W. Meijer, *Chem. Eur. J.*, 1997, **3**, 300-307.
28. J. W. Steed, *Chem. Commun.*, 2011, **47**, 1379-1383.
29. C. S. Hawes, N. F. Chilton, B. Moubaraki, G. P. Knowles, A. L. Chaffee, K. S. Murray, S. R. Batten and D. R. Turner, *Dalton Trans.*, 2015, **44**, 17494-17507.